BBA - Molecular and Cell Biology of Lipids 1863 (2018) 1082–1094

Contents lists available at ScienceDirect

BBA - Molecular and Cell Biology of Lipids

journal homepage: www.elsevier.com/locate/bbalip

Structural basis of the lipid transfer mechanism of phospholipid transfer protein (PLTP)

Meng Zhang[a], Xiaobo Zhai[a], Jinping Li[b], John J. Albers[c], Simona Vuletic[c,*], Gang Ren[a,*]

[a] The Molecular Foundry, Lawrence Berkeley National Laboratory, Berkeley, CA 94720, United States
[b] Department of Biomedical Science, Mercer University School of Medicine, Savannah, GA 31404, United States
[c] Northwest Lipid Metabolism and Diabetes Research Laboratories, Seattle, WA 98109, United States

ARTICLE INFO

Keywords:
PLTP
Phospholipid transfer protein
PLTP bound to HDL
PLTP bound to liposome
Electron microscopy
HDL
Liposome

ABSTRACT

Human phospholipid transfer protein (PLTP) mediates the transfer of phospholipids among atheroprotective high-density lipoproteins (HDL) and atherogenic low-density lipoproteins (LDL) by an unknown mechanism. Delineating this mechanism would represent the first step towards understanding PLTP-mediated lipid transfers, which may be important for treating lipoprotein abnormalities and cardiovascular disease. Here, using various electron microscopy techniques, PLTP is revealed to have a banana-shaped structure similar to cholesteryl ester transfer protein (CETP). We provide evidence that PLTP penetrates into the HDL and LDL surfaces, respectively, and then forms a ternary complex with HDL and LDL. Insights into the interaction of PLTP with lipoproteins at the molecular level provide a basis to understand the PLTP-dependent lipid transfer mechanisms for dyslipidemia treatment.

1. Introduction

Phospholipid transfer protein (PLTP) mediates the phospholipid transfer among lipoproteins, including high-density lipoproteins (HDL), low-density lipoproteins (LDL), intermediate density lipoproteins (IDL), very low-density lipoproteins (VLDL) and chylomicrons [1, 2]. Additionally, PLTP has been reported to have a unique function in remodeling HDL [3]. Since it is well known that the HDL cholesterol level is closely related to atherosclerosis and coronary artery disease (CAD) [4, 5], exploring the connection between PLTP and CAD is necessary. Some studies suggest that high PLTP activity may be a risk factor for CVD based on the increased PLTP activity reported in CAD patients and the inverse correlation between PLTP expression and the HDL level [6–9]. However, there are also opposite results, indicating that low PLTP activity is a marker for peripheral arterial disease (PAD) [10] and PLTP deficiency causes accumulation of cholesterol in the circulatory system and accelerates the development of atherosclerosis [11]. These controversial results about PLTP function in developing CAD motivated our study of the mechanism of PLTP-mediated lipid transfer among lipoproteins at the molecular level.

PLTP is a plasma glycoprotein with a molecular mass of ~81 kDa [12]. As a family member of the lipopolysaccharide (LPS)-binding/lipid transfer proteins, PLTP shares approximately 20% sequence identity with cholesteryl ester transfer protein (CETP) and bactericidal permeability increasing protein (BPI) [13, 14]. Due to the similar roles of PLTP and CETP as lipid transfer vehicles, many biochemical experiments have been performed comparing their similarities and differences [13, 15]. Unlike CETP, which primarily mediates net lipid transfer, including the exchange of cholesterol ester (CE) and triglycerides (TG) from HDL to triglyceride-rich lipoproteins such as LDL [16], PLTP is mainly responsible for promoting the transfer of phospholipids from lipid-rich lipoproteins to HDL [17]. Both PLTP and CETP enable the remodeling of the HDL size, even without the involvement of another lipoprotein species [18, 19]. Moreover, incubation experiments in vitro have predicted that both PLTP and CETP could form a ternary complex with two HDL particles, creating a large unstable fusion intermediate, which would finally result in either three smaller particles or remain as an enlarged fusion particle [19, 20]. However, electron microscopy experiments did not favor this hypothesis, at least for CETP, due to the absence of observation of the ternary HDL-CETP-HDL complexes [21–24]. Whether the ternary complex of HDL-PLTP-HDL could be observed by electron microscopy remains a question.

Although the structure of PLTP is still unavailable, homology models have been constructed based on the X-ray structure of human BPI [25–27]. PLTP was predicted to have a banana-shaped structure with a long narrow tunnel connecting two distal end openings and two lipid binding pockets [25], which is very similar to the structure of CETP [25]. However, the Ω1 flap on the C-terminal end of CETP [28]

* Corresponding authors.
E-mail addresses: simona@uw.edu (S. Vuletic), gren@lbl.gov (G. Ren).

https://doi.org/10.1016/j.bbalip.2018.06.001
Received 16 January 2018; Received in revised form 10 May 2018; Accepted 1 June 2018
Available online 05 June 2018

end adopts a very different conformation to that in PLTP. Moreover, two α-helixes along the PLTP tunnel are relatively short compared to those of CETP, potentially affecting the structural flexibility of PLTP. Considering that PLTP and CETP have different functions and activities during lipid transfer [15], it is necessary to investigate whether PLTP adopts a similar binding conformation with HDL as that of CETP, and whether it shares a similar lipid transfer mechanism to CETP, such as the shuttle mechanism [21, 29] or the tunnel model [30].

Difficulties in studying the structure-based PLTP-mediated lipid transfer and HDL remodeling mechanisms lie in lipoprotein structure heterogeneity [31–33], which is caused by the variety of lipoprotein compositions, such as difference in lipid and protein components among or within each species of lipoproteins. Moreover, the physical properties of the lipid components result in lipoprotein structural softness and dynamics, especially for HDL [34–36]. A particle-by-particle structural study is required to examine lipoprotein-PLTP interactions. Here, we used our reported and validated optimized negative-staining electron microscopy (OpNS EM) protocol [34, 37], rapidly settling the structure and eliminating the major artifacts [22, 38–40] without losing high contrast or structure details [34, 37, 41], to examine the example. We then used individual-particle electron tomography (IPET) [42] and single-particle analysis (SPA) techniques [43] to study the three-dimensional (3D) structure of PLTP and its interaction with lipoproteins and the liposome. As a comparison, CETP was also used for the incubation with different lipoproteins.

2. Results

2.1. Structure of PLTP

We first examined a PLTP sample using the optimized OpNS-EM methodology [19, 27]. Both the surveyed micrographs (Fig. 1A) and the selected particle views (Fig. 1B) revealed a boomerang- or banana-shaped structure of PLTP, as predicted by homology modeling [25], with dimensions of ~12.4 ± 1.9 nm × ~3.8 ± 0.6 nm. These measurements excluded aggregated particles, which may be related to the exposure of PLTP surface hydrophobic residues [44] to the solvent. As a comparison, a sample of mutated PLTP (M159E) [45], which lacks lipid transfer activity [5], was also examined (Supplementary Fig. 1A). Isolated particles of wild-type PLTP were windowed (Fig. 1B) and the particle images were submitted to reference-free classification and averaging [38]. The result showed that the particle shape and size are highly similar to the homology model (Fig. 1C) and some detailed features could be distinguished, such as the concave-shaped surface, the tapper N-terminal β-barrel domain and globular C-terminal β-barrel domain (Fig. 1C and D).

A further examination of the 3D structure and dynamics of the PLTP particles were conducted by electron tomography (ET). The targeted particles were imaged from a series of tilt angles ranging from −60° to 60° in steps of 2°. The images of each individual PLTP particle were extracted from the tilted series after contrast transfer function (CTF) correction, and then the particle tilt series were submitted for 3D individual-particle electron tomography (IPET) reconstruction [42] (Fig. 1E). Representative IPET 3D reconstructions (Fig. 1F, right six columns) and tilted views of representative particles (Fig. 1G) confirmed the banana-shaped structure of PLTP, with similar dimensions to the homology model [25]. The analysis of the curvature of IPET-reconstructed PLTP particles showed a noticeable variation in the angle between the two center axes of the N- and C-terminal β-barrel domains (with a mean of 140.63° ± 10.61°) (Fig. 1F, third row), which has been predicted by molecular dynamics simulations in CETP [46]. The resolutions of the IPET 3D maps were ~19 Å based on the intra-Fourier shell correlation (intra-FSC) analysis [42] (Fig. 1H, right panel).

To validate the significance of the IPET 3D reconstruction, the single-particle 3D reconstruction method was used to classify and average a total of ~7000 particle images [43]. In this process, the IPET 3D map was used as an initial model after low-pass filtration to 80 Å to avoid potential initial model bias. The single-particle 3D reconstruction at a resolution of ~19 Å confirmed the banana-shaped structure of PLTP (~129 Å × 36 Å), which is very similar to the IPET 3D reconstruction and the homology model (Fig. 1F, first column and last row). Fitting the homology model into the envelopes of the single particle 3D reconstruction showed a similar quality to that fitted to the IPET 3D reconstruction, suggesting similar resolution between the IPET and the single particle 3D reconstructions (Fig. 1H, left panel).

2.2. Binary conformation of the PLTP-HDL$_3$ complex

To examine how PLTP interacts with HDL$_3$, PLTP was incubated with HDL$_3$ at molar ratios of ~3:1, and then examined by OpNS EM. The survey EM images showed that protruding features were observed on the spherical-shaped HDL$_3$ particles (with an HDL$_3$ diameter of ~12.28 ± 1.91 nm) (Fig. 2B), in which no more than two PLTP molecules could be observed on a single HDL$_3$ particle (Supplementary Fig. 1G). In comparison, the HDL-PLTP$_{M159E}$ sample only had 1.88 ± 0.89% of the HDL$_3$ particles that were observed with protruding features, which is significant lower than the percentage of bound HDL$_3$ in the HDL-wild-type PLTP sample (25.06 ± 4.19%). This lower percentage of binding to HDL$_3$ may explain the ineffective lipid transfer activity [5] of PLTP$_{M159E}$. Interestingly, much less aggregation of the PLTP particles was observed compared with the sample of PLTP alone (Fig. 2A), which implies that the disassembling of the aggregates may occur through the absorption of PLTP onto HDL$_3$ particles. To analyze the detailed structure of PLTP-bound HDL$_3$, complex particle images were submitted to reference-free 2D classification and averaging (Fig. 2C and D). The class averages showed that the distal end of PLTP inserts into the HDL$_3$ particles, with ~8.09 ± 1.41 nm remaining outside the HDL$_3$ surface. The averaged PLTP width is ~3.44 ± 0.51 nm and the binding conformation is similar to the garlic-shaped structure of CETP binding to HDL$_3$ [31]. This result suggests that the hydrophobic N-terminal β-barrel domain of PLTP interacts with HDL$_3$.

To further examine the structure of PLTP-bound HDL$_3$ in 3D, PLTP-HDL$_3$ complexes were also imaged using OpNS ET (Fig. 2E). A series of tilt views of the images (ranging from −62° to +67° in steps of 1.5°) confirmed the garlic shaped structure (Fig. 2G), in which a banana-shaped PLTP molecule is attached to a spherical HDL$_3$ particle, as observed in 2D images. By using IPET, 3D density maps were reconstructed from the tilted images of individual complexes. Representative complex particles showed resolutions of ~27 Å (indicated by intra-FSC analysis) (Fig. 2H, right, and Fig. 2F, right four columns). The density contour level of these 3D maps was defined as close to a molecular weight of ~330 kDa, which confirmed the garlic-shaped 3D structure of the complex. Additionally, we detected a variety of HDL$_3$-PLTP complexes, especially in terms of the size of the HDL$_3$ particle (10.82 ± 1.43 nm) and the width of the free end of PLTP (3.39 ± 0.64 nm; Fig. 2F, last row).

To evaluate the statistical significance of the IPET 3D structures, the single-particle 3D reconstruction method [38] was also used to classify and average a total of ~32,000 complexes of PLTP-HDL$_3$ (Fig. 2F). As an initial model, the IPET 3D maps were low-pass filtered to 80 Å to avoid potential bias. Due to the heterogeneity of HDL$_3$, only a small portion of complexes (~4700 particles) with relatively homogeneous HDL$_3$ diameters were selected for 3D reconstruction (Fig. 2H, left panel). The single-particle 3D reconstruction at a resolution of ~23 Å again confirmed a garlic-shaped structure, with a quasi-spherical HDL$_3$ (with dimensions of ~11.5 × 11.6 × 11.6 nm) carrying a rod-shaped PLTP protrusion (with a length of ~8.0 nm and a width of ~3.8 nm, at a contour level corresponding to the molecular volume of the complex). This spherical HDL$_3$ contains a low-density core and a relatively high-density outer shell, whereas the density of the PLTP protrusion is even higher than the outer shell. The angle between the inserted PLTP and

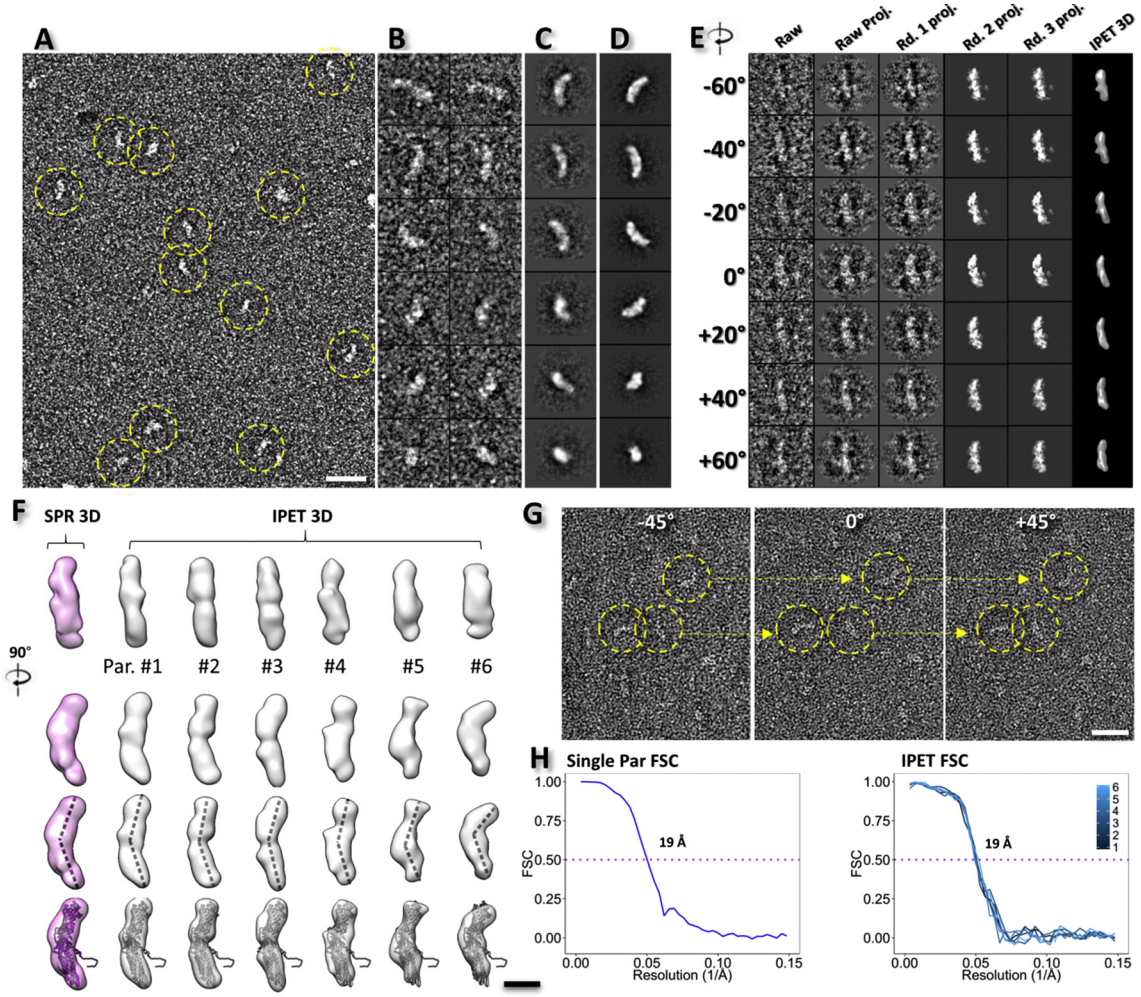

Fig. 1. OpNS EM images and 3D reconstruction of PLTP particles. A) Survey view of the sample of PLTP particles (yellow dashed circles). B) Representative raw PLTP particles. C) Selected reference-free class averages. D) Selected projections of the single particle 3D reconstruction (average from a thousand particles). E) Ab-initio 3D reconstruction of an individual PLTP particle by individual particle electron tomography (IPET). The particle was imaged by electron tomography (ET, tilt angles ranging from −60° to 60° in steps of 2°). Seven representative tilt views of a targeted PLTP particle present the step-by-step process of IPET 3D reconstruction shown in columns 2 to 5. The final IPET 3D reconstruction is displayed in the last column. F) The comparison of the single particle 3D reconstructions (column 1, pink model) and the IPET 3D reconstructions (columns 2 to 7, gray models). Six representative IPET 3D reconstructions from six targeted PLTP particles are displayed, with different curvatures indicated by docking of the homology model into each density map (row 4). G) Three representative tilt views of the single-axis tilt series of PLTP particles. H) The resolutions of the single particle 3D reconstruction and the resolution of the IPET 3D reconstruction are estimated by FSC between two models built from odd- and even-numbered views, respectively. Scale bars: A, 25 nm; F, 5 nm; G, 20 nm. The box sizes are 29 nm for B, C, D and E.

the tangent plane of the HDL_3 surface is ~63°, which is similar to that of CETP-bound HDL [31].

To determine the orientation of PLTP in binding to HDL_3, two structural analysis methods in Chimera [47] were used to analyze the PLTP homology model fitting into the protruded density on the HDL_3 surface (Fig. 2F, third row). Unfortunately, these analyses were insensitive to distinguish which distal end penetrates the HDL_3 surface. In detail, i) by fitting each of the β-barrel domains into the rod-shaped density portion, the average map fit value showed a similar score (~4.65 vs. ~4.69; and ~22.4% vs. ~18.2% atoms outside the contour for the C-terminal and the N-terminal fitting, respectively); ii) by computing the correlation values between the protrusion density and 14-Å-resolution density maps generated from the above two fittings, respectively, the R-value results of ~0.95 vs. ~0.94 were insufficient to distinguish which was better. However, considering the distal end of the N-terminal β-barrel domain contains a hydrophobic lipid pocket similar to CETP, and the CETP N-terminal β-barrel domain penetrates into the HDL_3 surface [21, 31] due to hydrophobic interactions [22], we hypothesize that the N-terminal pocket opening penetrates the HDL_3 surface.

2.3. Binary conformation of PLTP interacting with LDL, VLDL or Liposome

To examine the interactions between PLTP and other lipoproteins, such as LDL, VLDL, and liposome, the lipoprotein samples were incubated with or without the presence of PLTP, and then imaged using OpNS EM. Without PLTP, the spherical shaped particles of LDL (diameter ~200–300 Å), VLDL (diameter ~370–600 Å) and liposome (diameter ~200–1000 Å) showed no protrusions (Supplementary Fig. 1D, E and F). However, in the presence of PLTP, rod-shaped PLTP molecules were observed on the globular surface of LDL, VLDL and liposome (Fig. 3A, B and C). Approximately 7.3% of the LDL particles, ~4.3% of the VLDL particles and ~13% of the liposomes showed one or two protrusions (Fig. 2A and B, and Supplementary Fig. 1H). The angle between the inserted PLTP and the tangent plane of the LDL and VLDL surface is difficult to measure due to the large difference in diameters between LDL/VLDL and PLTP, and the much floppier 3D structure of LDL/VLDL compared with HDL_3. The percentages of particles bound to PLTP were significantly higher for HDL_3 than for LDL and VLDL, suggesting that PLTP has a higher binding affinity for HDL_3 than for LDL/VLDL/liposome.

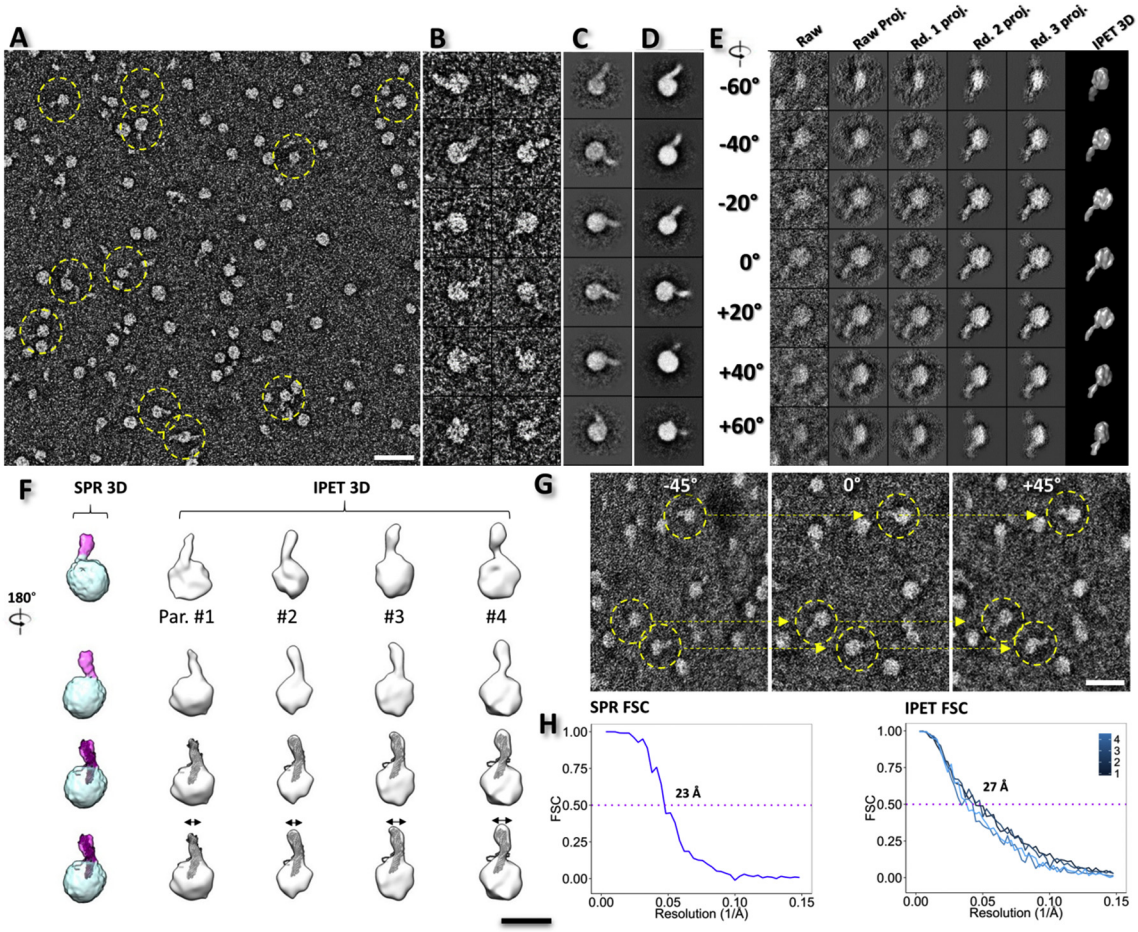

Fig. 2. OpNS EM images and 3D reconstruction of the PLTP-HDL_3 complexes. A) Survey view of PLTP-HDL_3 complexes, indicated by yellow dashed circles. B) Representative particle images of PLTP-HDL_3 complexes. C) The selected reference-free class averages. D) Selected projections of the single particle 3D reconstruction. E) Ab-initio 3D reconstruction of an individual PLTP-HDL_3 complex by IPET. The complex was imaged by ET tilting from −62° to 67° in steps of 1.5°. Seven representative tilting views (column 1) were compared to the projections from the intermediate 3D reconstruction (columns 2 to 5) at corresponding angles. The final IPET 3D reconstruction is displayed in the last column. F) The comparison of the 3D reconstructions by the single particle averaging method (column 1, a quasi-spherical shape density and a single protrusion were labeled with cyan and pink colors, respectively) and IPET (column 2 to 7, gray models). Four representative IPET 3D reconstructions of PLTP-HDL_3 complexes were docked with the homology model of PLTP (row 3). G) Three representative views of the single-axis tilt series of PLTP-HDL_3 complexes. H) Single particle 3D averaging and IPET 3D reconstruction resolution were estimated by Fourier-shell correlation (FSC) between two models built from odd- and even-numbered views, respectively. Scale Bars: A, 40 nm; F, 15 nm; G, 30 nm. All the box sizes are 37 nm for B, C, D and E.

2.4. Ternary conformation of PLTP interacting with HDL_3 and LDL, VLDL or liposome simultaneously

To examine how PLTP interacts with atheroprotective and atherogenic lipoproteins simultaneously, samples of the co-incubation of LDL with HDL_3 in the presence of PLTP were imaged using OpNS EM. The micrographs showed a small amount of LDL particles forming a ternary complex via the bridging of two HDL_3 particles through a PLTP molecule (Fig. 3D). The portion of bridges are ~25 Å, which is markedly shorter than the length of PLTP alone (~129 Å) or the length of the PLTP protrusion on the HDL_3 surface (~80 Å), suggesting that both distal ends of PLTP penetrated into the corresponding surface of LDL and HDL_3 simultaneously. When repeating the above experiments by co-incubating with VLDL or liposome, a similar phenomenon was observed, in which a rod-shaped PLTP density (with a length of ~30 Å) bridging a large spherically shaped VLDL or liposome with a small spherically shaped HDL_3 particle (Fig. 3E and F). Interestingly, the percentages of PLTP-bound LDL, VLDL and liposome particles were about doubled in forming the ternary complexes, i.e., ~16.6%, ~11.9%, and ~18.2%, respectively. A similar phenomenon was also previously observed for CETP-lipoprotein incubation [23], which suggests that CETP and PLTP share a similar binding mechanism. The interaction of the N-terminal β-barrel domain with HDL_3 may trigger a conformational change in the C-terminal β-barrel domain to increase the binding affinity to other lipoproteins.

2.5. PLTP function in HDL_3 remodeling

To examine the differences in PLTP-mediated lipid transfer efficiency among HDLs themselves, between HDL_3 and other lipid-rich particles or merely fusing the HDL_3 particles, the above samples, HDL-PLTP-LDL/VLDL/liposome (with a molar ratio of PLTP, HDL_3 and LDL/VLDL/liposome of 9:3:1) and PLTP-HDL_3 (molar ratio of 3:1) were further incubated separately for up to 24–48 h at 37 °C. Samples without HDL_3 (LDL/VLDL-PLTP) or PLTP (HDL_3-liposome) were used as controls. The molar ratios of lipoproteins were estimated based on the protein concentration of apoA-I and apo-B in HDL and LDL/VLDL, in which it is assumed that the spherical HDL contains three copies of ApoA-I and LDL/VLDL contains one copy of ApoB-100. The molar ratios were further validated by EM images, in which the lipoprotein samples were mixed under different ratios and dilution conditions for TEM examination. The average number of particles per unit area on the carbon film was calculated to confirm the molar ratio in the original samples.

Since the amount of lipid transfer cannot be measured by OpNS EM,

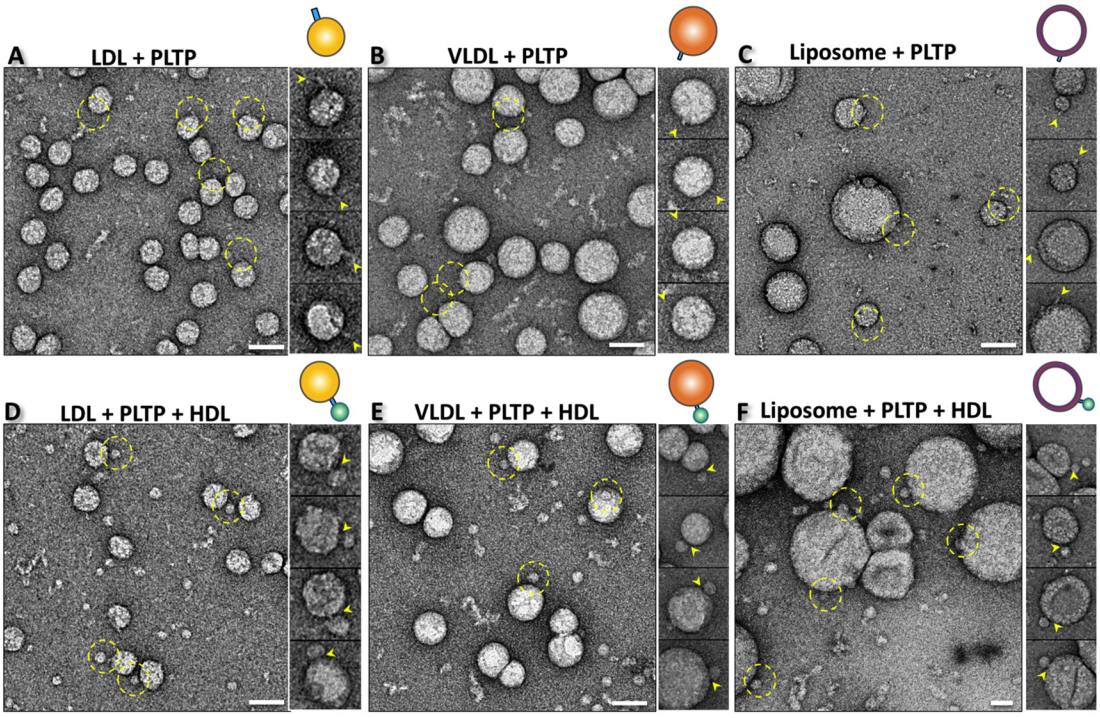

Fig. 3. Structure of PLTP bound to LDL, VLDL and liposome by OpNS EM. Survey OpNS EM images (left panel), representative particle images (right panel) and the corresponding particle cartoon (top right panel) of the binary complex after incubating PLTP with A) LDL, B) VLDL, or C) liposome and the ternary complex after incubating HDL_3 and PLTP with D) LDL, E) VLDL, or F) liposome at 37 °C for 1 min. The PLTP binding positions on each type of substrate were labeled with yellow dashed circles and yellow arrows. Particle window size: A, 44 nm; B, 60 nm; C, 120 nm D, 44 nm; E, 74 nm; F, 96 nm. All scale bars: A–F, 40 nm.

the change in the HDL_3 diameter was used as an alternative to indirectly reflect the lipid transfer activity from lipid-rich particles to HDL_3. The observation of HDL size change in this simplified model can also be affected by the PLTP-mediated fusion process [48]. At certain point, pre-β particles are released, and the remaining apoA-I deficient HDL_3 particles are prone to fuse thereby increasing particle diameter. Therefore, the increase in particle size is not a perfect surrogate for PLTP transfer activity.

Starting with a relatively simple case, in which only HDL_3 and PLTP were incubated at a molar ratio of 1:3, OpNS EM images showed an increased HDL_3 size with incubation time (Fig. 4A, Supplementary Fig. 2A and B). In brief, although the HDL_3 size remains stable at 15 min and 40 min, a significantly increased HDL_3 size (~110%) was observed after a two-hour incubation (Fig. 4E), and it grows continually until 8 h with its diameter increased to ~135% compared with the initial conditions. Meanwhile, the number of HDL_3 particles showed an observable decrease. After 8 h, the growth started to slow down. This may be due to the lack of free volume, which will not allow more lipids to be loaded onto the surface of a large HDL_3 particle. The largest particle at 24 h was approximately 4 times larger in diameter than normal HDL_3. In these experiments, the ternary complex of one PLTP bridging two HDL_3 particles was not observed.

As a control, LDL and PLTP were also incubated together at a molar ratio of 1:3. The particle size measurement from OpNS EM images showed that the LDL size remains at 100% (~25.5 nm) over the whole incubation time up to 24 h, suggesting that PLTP does not cause any significant size variation in the LDL particle (Supplementary Fig. 2C and D).

2.6. Comparison of PLTP and CETP functions in HDL_3 remodeling

To further understand the functional specificity of PLTP in remodeling the HDL_3 size, we repeated the above experiments using CETP to compare with PLTP (Fig. 5). The statistical analyses of the HDL_3 size from the OpNS images showed that: i) PLTP-mediated HDL_3 remodeling was much slower than that by CETP. The peak HDL_3 size shifted away from its original position at 8 h for PLTP, while it took only 2 h for CETP to produce a noticeable HDL_3 size change; ii) PLTP-mediated remodeling led to a general increase in the HDL_3 size, which results in a more homogenous population. Small particles are rarely observed in the images of the PLTP-HDL_3 samples. In comparison, the density of the HDL_3 size peak decreased dramatically after 40 min for CETP but not PLTP, and the peak split at 8 h, indicating that CETP redistributed the HDL_3 population and most of the particles centered on a smaller size. iii) Though both PLTP and CETP can cause the formation of large HDL_3 particles, the HDL_3 particles enlarged by PLTP have a much "smoother" surface, while CETP-induced large HDL_3 particles are generally attached to multiple CETPs, indicating differences in the mechanisms of HDL_3 remodeling by PLTP and CETP.

2.7. PLTP-mediated lipid transfer between HDL_3 and LDL/VLDL/Liposome

To study the PLTP-mediated lipid transfer function in the presence of both atheroprotective and atherogenic lipoproteins simultaneously, we incubated LDL, HDL_3 and PLTP together at a molar ratio of 1:3:9 for different lengths of incubation time. OpNS EM images showed that the mean diameter of the HDL_3 increased with incubation time for the HDL_3-PLTP-LDL sample (Fig. 4B). In brief, although the HDL_3 size (~10.3 nm in the beginning) was not significantly changed after incubation for 15 min and 40 min, the mean diameter increased to ~108% of the initial diameter after 2 h (Fig. 4B and E, Supplementary Fig. 3A and B) and further increased to ~132% after 24 h. This performance was similar to the increase in the HDL_3 size in the absence of LDL, suggesting that LDL is not a major factor that influences the rate of HDL_3 size growth. Similarly, we compared the HDL_3-PLTP-LDL incubation to the previously reported incubation of HDL_3-CETP-LDL (Supplementary Fig. 4) [23], where the HDL_3 size peak did not diverge as shown in the CETP-HDL_3 incubation (Fig. 5A and C). However, in the

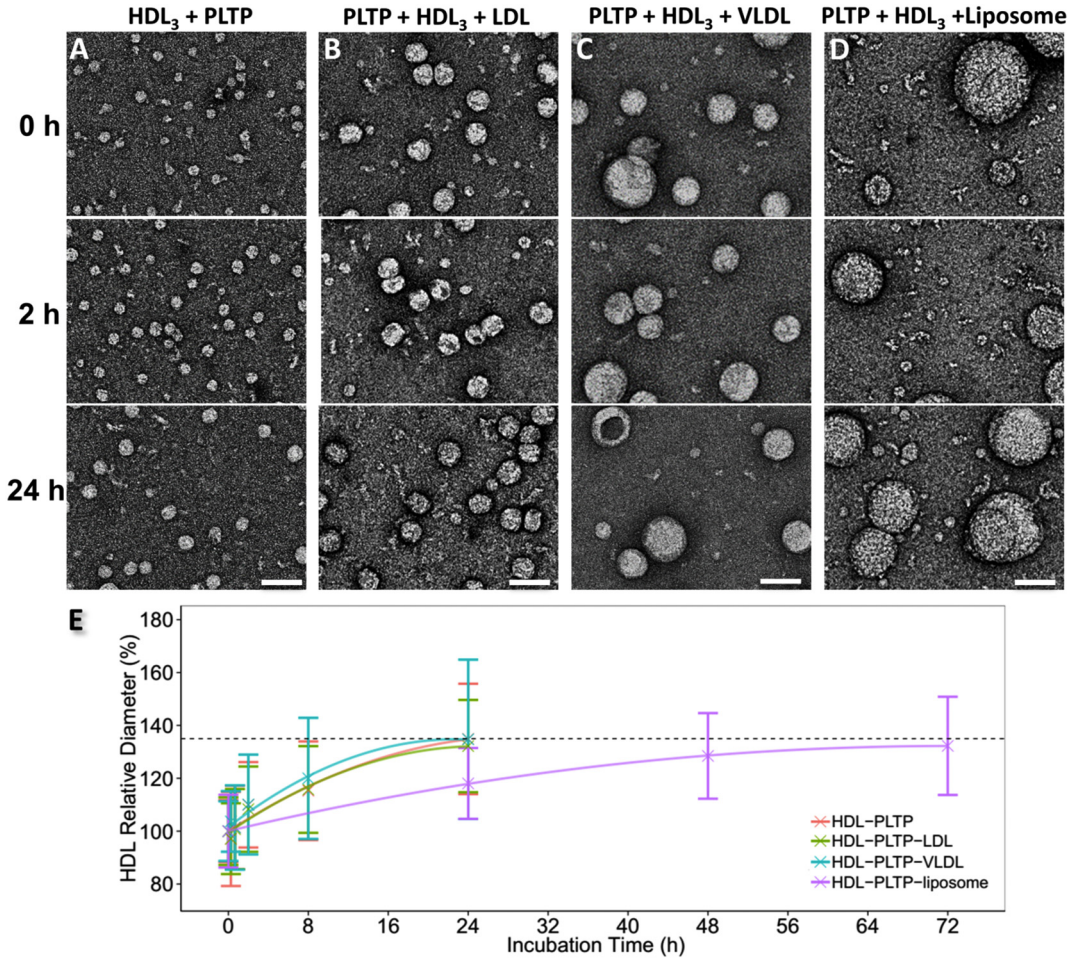

Fig. 4. PLTP-induced HDL_3 remodeling in the samples of HDL_3-PLTP, HDL_3-PLTP-LDL, HDL_3-PLTP-VLDL and HDL_3-PLTP-liposome. A) OpNS EM images of the sample of HDL_3, B) HDL_3 and LDL, C) HDL_3 and VLDL, and D) HDL_3 and liposome were incubated with PLTP at 37 °C for an incubation time of 0 h, 2 h and 24 h (for HDL_3-PLTP, HDL_3-PLTP-LDL and HDL_3-PLTP-VLDL) and 0 h, 24 h and 72 h (for HDL_3-PLTP-liposome). E) The statistical distribution of HDL_3 size against the incubation time. Approximately 300–500 HDL_3 particles were assessed for each category. The relative mean diameter measurement of HDL_3 starting at 0 min (~12.50 nm) is set as 100%. The particle diameters were measured based on the geometric mean of two diameters: the longest diameter and its perpendicular diameter. All scale bars: 50 nm.

presence of LDL, the larger "spiky" particles (the particles attached to multiple PLTPs) disappeared and the HDL_3 particle size continued declining (Supplementary Fig. 4). This significant difference between PLTP and CETP indicates that CETP-mediated HDL_3 remodeling is more dependent on other species of lipoproteins. This activity is consistent with the observation that a higher percentage of LDL/VLDL particles showed bound CETPs [23] compared to bound PLTPs (Fig. 3A and B).

As a parallel comparison experiment, VLDL instead of LDL was used to repeat the above experiments (HDL-PLTP-VLDL) (Fig. 4C and E, Supplementary Fig. 3C and D). The OpNS EM images showed that the HDL_3 sizes increased to ~110% and ~134% at 2 h and 24 h, respectively. The fitted curve was similar to that of HDL_3-PLTP and HDL_3-PLTP-LDL, as described above (Fig. 4E). These results confirm that the rate of PLTP-mediated HDL_3 growth is also not significantly altered by VLDL.

Similar to the above, liposome instead of LDL/VLDL was used to repeat the incubation experiments (HDL_3-PLTP-liposome). Liposomes are well-defined phospholipid donors to HDL_3, designed to measure the phospholipid transfer activity by radioactive labeling [49, 50]. The samples of liposome particles were incubated with HDL_3 particles with or without PLTP at a molar ratio of 1:3:9 (liposome:HDL_3:PLTP) or 1:3 (liposome:HDL_3), respectively. The control samples without PLTP showed that the HDL_3 particles retained a constant size during long-term incubation (Supplementary Fig. 5A). In the presence of PLTP, the mean diameter of the HDL_3 particles increased throughout the incubation time (Fig. 4D and E). However, the speed was slower than for LDL/VLDL. For example, after 24 h, the particle size only increases to ~120%, similar to the size increase in the VLDL/LDL-PLTP-HDL_3 experiment in 8 h. To achieve a similar final HDL_3 particle size of ~135%, as seen in the VLDL/LDL-PLTP-HDL_3 experiments at 24 h, the liposome-PLTP-HD_3L sample incubation had to be extended to 72 h (~132% of the initial size) (Fig. 4D, Supplementary Fig. 5B).

Based on the evidence from the above incubation experiment that the HDL_3 size increase rate is similar in both the HDL_3-PLTP and the HDL_3-PLTP-LDL/VLDL groups, we can conclude that PLTP-induced HDL_3 self-remodeling has greater effect on the HDL_3 size compared with lipid transfer from other lipoprotein species to HDL_3. This is in agreement with the observation that liposome slows down the PLTP-mediated HDL_3 remodeling. Given that more PLTPs bound to liposome than to LDL and VLDL (~13% for liposome vs. 7.3% for LDL and 4.3% for VLDL bound to PLTPs, plus each liposome can bind more PLTPs due to its large surface area), a lower percentage of PLTP will participate in the HDL_3 self-remodeling, although it may increase the formation of ternary complexes for lipid transfer. However, the effect of the latter is much weaker than the former.

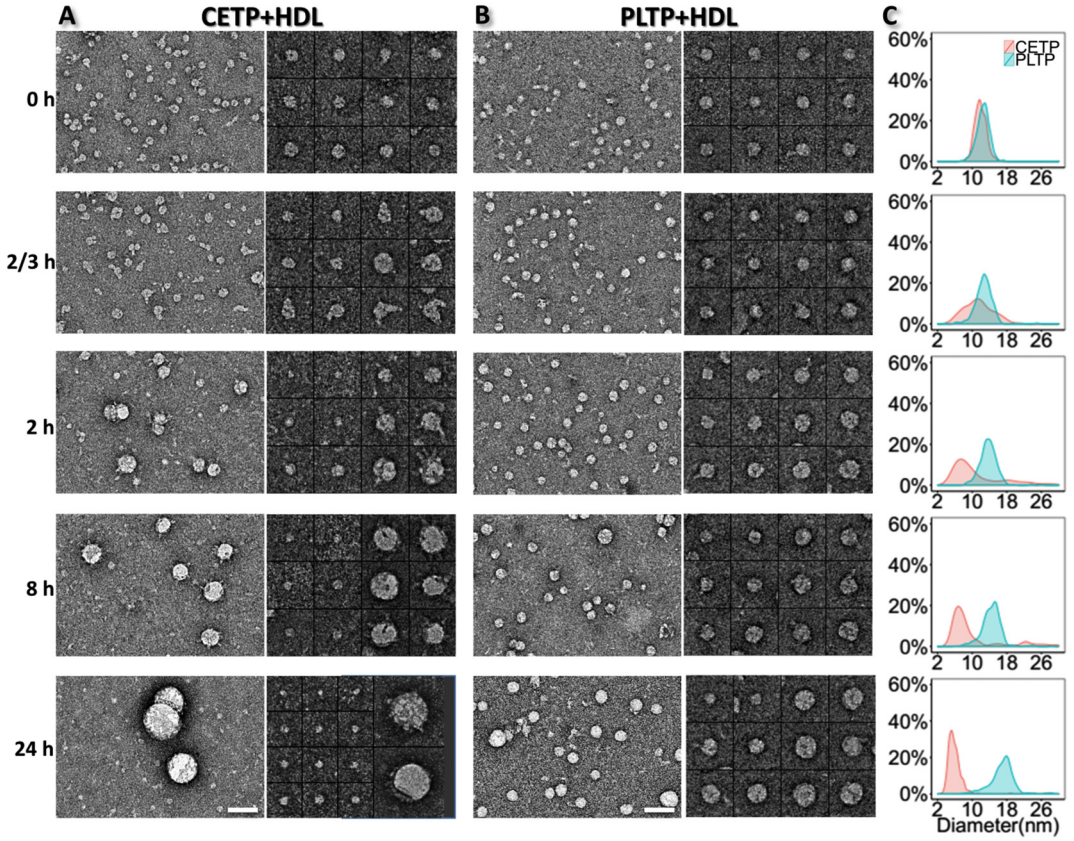

Fig. 5. Comparison of the HDL_3 remodeling process by PLTP and CETP. A) OpNS EM images (left panel) and selected particles (right panel) of CETP incubated with HDL_3 samples after an incubation of 0 min, 15 min, 40 min, 2 h, 8 h and 24 h at 37 °C. B) The OpNS EM images and selected particles of PLTP incubated with HDL_3 with the same time series and temperature. C) The statistical analysis of the HDL_3 size distribution at each time point. A different peak shift direction can be observed in the two groups. The molar ratios of HDL_3 vs. CETP/PLTP were both set at 1:3. Scale bars: A and B, 50 nm. Box sizes A and B, 37 nm. For 24 h, the box sizes are 28 nm and 55 nm, respectively.

3. Discussion

3.1. The structure of PLTP determined by the OpNS IPET method

Since the discovery of PLTP and its cloning in 1994 [10], numerous questions about its 3D structure and the nature of its interactions with lipids and lipoproteins have remained unanswered because of the technical difficulties associated with the crystallization of PLTP and the direct observation of its interactions with lipoprotein particles. Using our OpNS protocol [34, 37], the IPET approach [42], and a conventional single-particle reconstruction approach, we visualized the 3D molecular structure of PLTP and its interactions with various lipoproteins. The observed 3D structure of the PLTP molecule revealed by the studies reported here remarkably resembles the homology model based on the BPI crystal [25–27], including the previously putative model of an allegedly disordered portion of the C-terminal tail-end sequence of PLTP, not seen in any of the other molecular family members. These studies confirm the two β barrel-like domains containing the N- and C-terminal lipid binding pockets (and their relative positions), the curvature of the banana-shaped molecule, and the presence of a channel through the entire length of the molecule.

In addition to individual PLTP molecules, we also observed PLTP molecular aggregates. These aggregates may be the inactive form of the PLTP, which represents up to 70% of all PLTP in human blood, and have an average size distribution from 340 to over 600 kDa [51–53]. Interestingly, a PLTP mutant that is inactive in lipid transfer, $PLTP_{M159E}$, formed more aggregates than wild-type PLTP and had even fewer interactions with HDL, supporting the idea that some of the lipid transfer inactivity may be associated with self-aggregation of PLTP molecules and their inability to bind lipoproteins.

The concepts of active and inactive PLTP refer to PLTP found in the blood. Recombinant PLTP is not bound to lipoproteins (the presumed basis of active PLTP in the blood. The self-aggregated forms in the rPLTP preparation are rare and contain no other proteins, such as those found in the inactive PLTP complexes in the blood. Therefore, it is not possible to compare rPLTP with the so-called active or inactive forms of PLTP in the blood. Even if some inactive form of PLTP is present, it is unlikely that it would introduce a bias in our observations.

3.2. The PLTP-HDL complex is the basic functional unit for lipid transfer activity

The observation of a clear rod-shaped protrusion adopting a vertical conformation relative to the HDL_3 surface is direct evidence that PLTP is part of the binary complex binding to the HDL_3 surface. No PLTP molecule was found with its concave surface docking to the convex surface of HDL_3, or with its two distal ends bridging two HDL_3 particles, together forming a typical “dumbbell” shaped ternary complex. This observation of the convex surface of PLTP binding to HDL_3 implies that that PLTP binding to HDL_3 particles is directional. The observation of fewer $PLTP_{M159E}$-HDL_3 complexes suggests that mutation may disable this HDL_3 binding function of PLTP either directly (by changing the PLTP structure) or indirectly (by enhancing PLTP aggregation). Overall, fitting the PLTP model into the binary complex showed consistency between the structure and the density map. However, the free C-terminal globular end of the PLTP was larger than expected. Since one function of PLTP is the delivery of phospholipid molecules from the HDL_3, this extra electron density may be related to accumulated

phospholipid molecules around the surface of the PLTP C-terminus, as we observed a similarly enlarged PLTP protrusion in the 2D images (Fig. 2).

Our data suggest that the portion of PLTP that penetrates into the HDL_3 surface represents ~35% of the molecule, most likely representing the N-terminus of PLTP. The free end of PLTP seems more likely to be the globular and curved C-terminus of the PLTP molecule. These findings suggest that, under physiological conditions, the distal PLTP N-terminal end penetrates into or through the phospholipid portion of the HDL_3 surface. The enlarged, rounded C-terminus may be associated with the initiation of the lipid transfer activity. Considering that the thickness of the monolayer of the lipid shell of phospholipids is ~28 Å, and the inserted portion of the PLTP molecule is markedly larger (~50 Å, Fig. 2F), the PLTP N-terminus could reach through the phospholipid layer and deep into the cholesteryl ester core of HDL_3. PLTP penetrates particles at an angle, which differs for the N- vs. the C-terminal. Therefore, although the length of PLTP molecule immersed into the HDL particle is approximately 40-50 Å, the actual depth PLTP molecule reaches within the particle is shorter. We assume that the position of the N-terminal pocket requires insertion into HDL at the specified length and angle for the lipid-binding pocket to become accessible.

Whether the HDL surface apolipoproteins especially apoA-I are involved in the interaction with PLTP is still unclear. One possibility is that PLTP directly interacts with the N-terminal of apoA-I HDL [54]. Other evidence showed that increasing the amount of apoA-II, which displaces apoA-I from HDL particles, decreases PLTP activity, and hinders the increase in HDL particle size [55, 56]. Another possibility is that, similar to CETP, the surface lipid mediates the PLTP bound to lipoprotein and liposome without apoA-I [22], in which smaller size of HDL particles showed more curvature and more hydrophobicity resulting more binding CETPs. Unfortunately, our approach and resolution are not able to distinguish these mechanisms.

PLTP can interact with HDL_3, LDL, VLDL and PL-liposomes both separately and simultaneously in binary complexes. However, PLTP has higher affinity for binding HDL_3 than apoB-containing lipoprotein particles. We presume that PLTP binds to the apoA-I and apoB-containing particles using the N-terminal of PLTP when binding only to a single lipoprotein species. Whether LDL/VLDL-bound PLTP is released from the complex in the presence of HDL_3 due to the affinity differences is unclear. More experiments are required to test this possibility, such as immune-EM experiment to identify the orientation of PLTP binding by designing antibodies against the distal ends of PLTP N- and C-terminal β-barrel domains.

Comparing the binding percentages of LDL, VLDL or liposome to PLTP after introducing HDL_3 into the solution, it is clear that the percentage of particles bound to PLTP increased (~16.6%, ~11.9%, and ~18.2%, respectively), which implies an allosteric regulation of PLTP after binding to HDL_3. The coexistence of ternary complexes of HDL_3–PLTP–LDL, HDL_3–PLTP–VLDL and HDL_3–PLTP–liposome is consistent with the mechanistic model of lipid transfer through a tunnel within the PLTP molecule. However, the low percentage of these complex particles implies that the interaction might be an instantaneous process or at least not stable. The observation of the ternary complex does not exclude the coexistence of a shuttle mechanism. Other experimental approaches, such as asymmetrical flow field−flow fractionation (AsFlFFF) showed that part of 35S-labeled PLTP initially binding with small unilamellar vesicles migrate into HDL population after 45 min incubation [57], These data are in agreement with a higher likelihood of observing the PLTP-HDL_3 binary complex than the PLTP-LDL/VLDL/liposome binary complex, suggesting that PLTP molecules generally prefer to attach to the HDL_3 surface.

The LDL sample (d = 1.006–1.069 g/ml, apoB 64.9 mg/dL) may include a small fraction of IDL particles and/or VLDL remnants ($1.006 < d < 1.019$ g/ml). Considering the LDL were isolated from healthy individuals with low triglyceride levels, our experience suggests that < 5% of the β-migration particles would constitute remnants. Furthermore, based on the particle diameters we did not observe other distinguishable population of particles by EM (Supplementary Fig. 1D). However, we cannot exclude the possibility that a small fraction of IDL interact with PLTP.

3.3. Comparing the HDL_3 remodeling dynamics between PLTP and CETP, generalizing the HDL_3 self-remodeling mechanism

PLTP and CETP both belong to a family of lipid transfer proteins. Here we list the similarities and differences after comparing the current PLTP study with an earlier CETP study [21, 22]. The similarities include: i) PLTP and CETP both show a banana-shaped structure; ii) both PLTP and CETP can insert into the surfaces of HDL_3, LDL, VLDL and liposome by using one distal end of a β-barrel domain, forming a binary complex; iii) both PLTP and CETP can form a ternary complex between different classes of lipoproteins (such as HDL_3 vs. LDL; HDL_3 vs. VLDL and HDL_3 vs. liposome). However, neither PLTP nor CETP can form a ternary complex within the same class of lipoproteins. The differences include: i) One of the major known functions of PLTP is to regulate the HDL_3 size and composition [58]. We observed marked differences in the dynamics and the form of HDL_3 modifications by PLTP and CETP. The comparison experiment of PLTP/CETP-induced HDL_3 self-remodeling showed that the PLTP-induced HDL_3 remodeling speed is much slower in terms of the HDL_3 size change compared to CETP (see the detailed discussion in the next section). In addition, the final product of the incubation with CETP included two populations of HDL_3 particles, ~6 nm smaller particles and large “spikey” particles, which were not observed in the incubation with PLTP; ii) Comparing the incubation of HDL_3-PLTP, HDL_3-PLTP-LDL, and HDL_3-PTLP-VLDL, we noticed that the HDL_3 size change did not show a significant difference with or without LDL/VLDL (Fig. 4A–C). This suggests that PLTP-mediated HDL_3 self-remodeling is the major function of PLTP in remodeling HDL_3. However, in the same experiment CETP showed that the addition of LDL to an HDL_3-CETP mixture can limit the generation of large HDL_3 particles (Supplementary Fig. 4), which suggests that CETP-mediated HDL_3 remodeling is more dependent on the lipid transfer between HDL_3 and LDL comparing to PLTP; iii) in our studies of CETP [21, 22], we reported that more than five CETP molecules can bind to a single plasma HDL_2 particle. In contrast, no more than two PLTP molecules bound to HDL_3. It is plausible that the binding of PLTP to HDL_3, like that of CETP, is a result of a hydrophobic interaction between PLTP and HDL [22]. However, the N-terminus of PLTP is known to interact with and bind to apoA-I [54], the main apolipoprotein in HDL_3 particles. It is, therefore, possible that protein-protein interactions together with hydrophobic interactions determine the number of PLTP molecules bound to HDL_3.

3.4. Hypothesized models for the mediation of HDL_3 self-remodeling by CETP and PLTP

Our observations are insufficient to provide a full picture of how CETP and PLTP coordinate the transport of lipids and transformation between HDL_3 and other types of lipoproteins. However, for a relatively simple system of HDL_3-PLTP/CETP, the above comparisons provide some useful hints to understand the HDL_3 self-remodeling mechanisms by PLTP/CETP.

Following the previous study of CETP-mediated CE/TG transfer between HDL_3 and LDL [21], two mechanistic models of HDL_3 self-remodeling by CETP and PLTP can be proposed: i) the tunnel model [29], where PLTP/CETP acts as a bridge between two HDL_3 particles, facilitating the lipid transfer; and ii) the shuttle model [30], in which PLTP/CETP acts as a vehicle that transfers lipids from one HDL_3 particle to another HDL_3 through the aqueous phase. Both models were plausible given the known functions of PLTP/CETP. However, in the tunnel model, we should observe one PLTP/CETP bridge between two HDLs to

form a “dumbbell” structure. Unfortunately, the absence of observation of these ternary complexes while imaging thousands of complexes does not support the tunnel mechanism. For a shuttle model, the shrinkage of part of the HDL_3 population must be followed by the enlargement of the remaining population. Though we observed a large variation in the HDL_3 size caused by both PLTP and CETP, almost all the HDL_3 particle sizes were increased by adding PLTP. Moreover, this model is difficult to explain how PLTP/CETP could directionally transfer lipids among the same species of HDLs. More than half of the CETP naturally appeared on the surface of HDL_3, which is less likely to support the shuttle model.

Absent of full support for either mechanism forced us to consider of another possibility. As a small functional unit, the HDL_3-PLTP/CETP complex must interact with other HDLs to generate the observed size variation. If this interaction is not caused by a PLTP/CETP bridge or shuttle, then it must be induced by HDL_3 itself. Since HDL_3 alone does not show a size variation after a sufficiently long incubation time (Supplementary Fig. 1C), the HDL_3 variation in the presence of PLTP/CETP must be caused by PLTP/CETP mechanisms. These detailed mechanisms about how PLTP/CETP remodeled the HDL_3 size were unknown. To study these mechanisms, we carefully examined the images. In addition to the above observations that large particles bound to many CETPs but rarely bound to PLTP, and that small globular particles (likely the small particles) appeared in the background of the CETP-HDL_3 samples but rod-shaped particles (likely PLTP particles) appeared in the background of the PLTP-HDL_3 samples, we also unexpectedly found a “triangular-shaped” interaction conformation in many complexes of CETP-HDL_3, especially in the initial stage of incubation (Fig. 6A). These “triangular-shaped” interactions did not clearly appear in the complexes of PLTP-HDL_3. In contrast, large HDL_3 surfaces were relatively smooth in the presence of PLTP. However, a small bulb was found in the far distal end of PLTP in many PLTP-HDL_3 complexes (Fig. 6B), which was not clearly seen in the CETP-HDL_3 complexes. These differences may reflect different mechanisms for PLTP and CETP.

We hypothesize that the HDL_3 remodeling mechanism of CETP mainly involves the transfer of lipids from the HDL_3 core to the HDL_3 surface through the central lipid pore to the concave surface of CETP, which leads to the formation of a triangle shape (Fig. 6C, first two rows). When more CETP particles insert into the HDL_3 surface, more imperfections may appear on the outer phospholipid surface of HDL_3, causing more hydrophobic interactions and a greater opportunity to fuse with other HDL_3-CETP complexes to form large particles. The number of CETP on the large HDL surface shall keep increasing as more HDL_3-CETP complexes are incorporated. However, the balancing process of the HDL_3 surface pressure may result in apolipoprotein separation from the merged HDL_3 (Fig. 6C, last two rows). In comparison to CETP, PLTP has a lower binding number to HDLs, resulting in the presence of more PLTP in the sample background (Fig. 6D, last two rows). We hypothesize that the PLTP mechanism of HDL_3 remodeling mainly involves the transfer of phospholipids from the HDL_3 surface to the distal end of PLTP (Fig. 6D, first two rows). The transfer of lipids to the outside of HDL_3 by PLTP would also cause the exposure of more hydrophobic components, destabilizing the original HDL_3 structure. The merging of several HDL_3-PLTP complexes may cause the release of the bound PLTP molecules. The HDL_3 remodeling also includes the release of surface apoA-I-PL pre-β molecular complexes from the HDL_3 particles and ensuing further fusion of the remaining apoA-I deficient HDL_3 particles [48].

As a result, the HDL_3 particle transformation step induced by the bound PLTP/CETP may be the prerequisite for the initiation of HDL_3 particle merging [22, 59]. This explains why the HDL_3 size exhibits almost no change within the first 40 min for PLTP and 15 min for CETP (Fig. 5). The capture of the intermediate stage of PLTP/CETP-mediated destabilization of the HDL_3 particle provides direct evidence to support the proposed particle merging model for HDL_3 self-remodeling.

In summary, the EM 3D structure of PLTP supports the homology model of PLTP. PLTP has a similar interaction with HDL and LDL to that of CETP. However, the PLTP activity in HDL remodeling is slower than that of CETP and occurs via a different mechanism. The EM images of the interaction of PLTP with lipoproteins provide the first picture for understanding PLTP-mediated lipid transfer, relevant for treating dyslipidemia.

4. Methods

4.1. Synthesis and isolation of PLTP and lipoprotein

PLTP (~1.625 mg/ml) was isolated using the previously reported procedure [60, 61]. Briefly, a PLTP His-tagged construct was expressed in mammalian cells, isolated from the concentrated conditioned media, purified, and stored at −80 °C until use. The purity of the isolated PLTP was evaluated by mass spectrometry, and no significant contaminants or other proteins were found in the isolated material. Wild-type plasma HDL_3 was isolated from fresh human plasma using ultracentrifugation as previously described [62]. It contained 4.28 mg/ml protein, 2.39 mg/ml CE and 1.03 mg/ml TG. LDL (d = 1.006–1.069 g/ml, apoB 64.9 mg/dL) and VLDL (d < 1.006 g/ml, apoB 24.5 mg/dL) were isolated in the Krauss laboratory by sequential flotation of plasma from fasted, healthy male volunteers and further purified by ultracentrifugation [63]. Liposome vesicle samples were produced by Encapsula NanoSciences (Brentwood, TN). The sample contained 1 mg/ml 1-Palmitoyl-2-oleoylphosphatidylcholine (POPC, from Avanti Polar lipids) with a peak vesicle size of ~50 nm in a buffer containing 20 mM Tris-Cl, 154 mM NaCl, at pH 7.4.

4.2. EM specimen preparation by the optimized NS (OpNS)

Conventional cryo-EM is often used for protein structural studies under physiological conditions since it avoids the potential artifacts induced by fixatives and stains [37]. Still, cryo-EM studies of PLTP are challenging; small molecules (< 150 kDa) are difficult to image or reconstruct using the cryo-EM single-particle approach because of low contrast [64]. Thus, we studied human PLTP using the OpNS protocol [34, 37]. Our OpNS protocol, refined from the conventional negative-staining protocol, eliminates rouleaux artifacts of lipoprotein particles and has been statistically validated as a way to determine lipoprotein particle shapes and sizes [34, 37].

Both the PLTP and PLTP-lipoprotein/liposome complex samples were prepared with the optimized NS protocol (OpNS) [37]. The PLTP was either directly diluted 1000 times (final concentration 1.625 μg/ml) with Dulbecco's phosphate-buffered saline (DPBS: 2.7 mM KCl, 1.46 mM KH2PO4, 136.9 mM NaCl, and 8.1 mM Na2HPO4; Invitrogen) buffer for PLTP Single Particle and IPET 3D reconstruction or co-incubated with HDL_3 at a molar ratio of 3:1 for PLTP-HDL_3 complex 3D reconstruction. LDL, VLDL and liposome were also co-incubated with PLTP and HDL_3 at molar ratios of 9:3:1 (PLTP:HDL_3:LDL/VLDL/liposome) with their original buffer at 37 °C for studying the PLTP-mediated lipid transfer activity among lipoproteins/liposome. To examine complexes at different time intervals, samples from the original incubation solution were fast fixed at 0 min, 15 min, 40 min, 2 h, 8 h, and 24 h on a carbon grid following the OpNS protocol. In brief, an aliquot (~3 μl) was placed on a thin-carbon-coated 200 mesh copper grid (Cu-200CN, Pacific Grid-Tech, San Francisco, CA) that had been glow-discharged. After ~1 min, the excess solution was blotted with filter paper, followed by a procedure of washing and staining as described [34, 37]. Three drops of 1% (*w/v*) uranyl formate (UF) negative stain on parafilm were then applied successively before being nitrogen-air-dried at room temperature. Since the UF solutions are light sensitive and unstable, this operation was performed in the dark [34, 37].

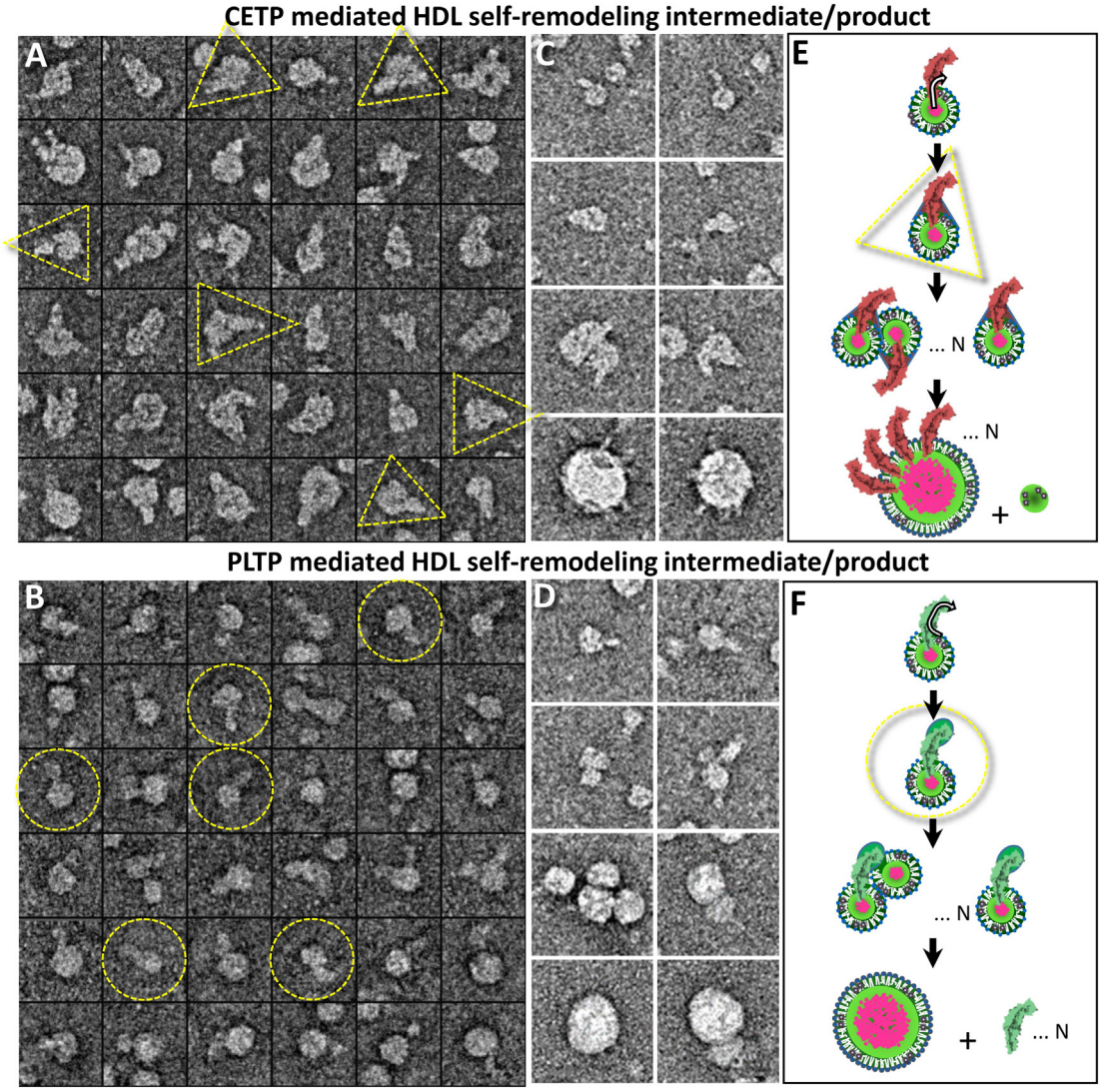

Fig. 6. Hypothesized mechanism of PLTP/CETP-mediated HDL_3 self-remodeling A) Selected particle views of CETP-bound HDL_3 showed a "triangular" shaped complex at the initial stage of CETP-HDL_3 incubation. B) Selected particle views of PLTP-bound HDL_3 showed an "enlarged free tapper end" of PLTP at the initial stage of PLTP-HDL_3 incubation. The yellow dashed circle and triangle mark out the free terminal end of PLTP and the CETP-HDL_3 complex, respectively. C and D) Hypothesized mechanism of CETP- and PLTP-mediated HDL_3 self-remodeling. Selected particles of the HDL_3-CETP/PLTP complexes shown in the left panel. Schematic of PLTP remodeling of HDL_3 through three stages: i) the formation of an unstable HDL_3-CETP/PLTP complex, ii) HDL_3-CETP/PLTP complex merging and iii) re-stabilizing, which results in different appearances of enlarged HDL_3 due to the amount of lipid transfer protein binding. CETP, PLTP, phospholipid, neutral lipids and ApoA-I molecules are displayed in magenta, green, white, pink and black, respectively. Box size: A and B, 37 nm; C and D, 62 nm.

4.3. Electron microscopy data acquisition and image pre-processing

The OpNS micrographs were acquired at room temperature under a defocus of ~0.6 um on a Gatan UltraScan 4 K × 4 K CCD equipped on a Zeiss Libra 120 Plus transmission electron microscope (Carl Zeiss NTS GmbH, Oberkochen, Germany). TEM was operated under a high-tension of 120 kV, energy filtering of 20 eV and 4 magnification range of 31.5 K to 80 K, in which each pixel of the micrographs corresponded to 3.68 to 1.48 Å, respectively. A total of ~230 micrographs were collected for the single particle reconstruction for the PLTP and PLTP-HDL_3 complex and ~10 micrographs were collected from each sample condition for the HDL-PLTP-LDL/VLDL/liposome incubation. The defocus of each micrograph was determined by fitting the contrast transfer function (CTF) parameters with its power spectrum using ctffind3 in the FREALIGN software package [65]. The phase of each micrograph was corrected by a Wiener filter with the SPIDER software package [66]. Approximately 200–500 particles from each ternary mixture sample at different time points were windowed and selected by the boxer software in the EMAN software package [43]. These particles are submitted for Gaussian low-pass filtering before statistical analysis.

4.4. Electron tomography data collection and image pre-processing

Electron tomography (ET) data of the PLTP and PLTP-HDL_3 specimens were acquired under a < 2 μm defocus with a high-sensitivity 4096 × 4096 pixel Gatan Ultrascan CCD camera at 80,000× magnification and with the same Zeiss Libra 120 TEM (each pixel of the micrograph corresponds to 1.48 Å). The specimens mounted on a Gatan 626 high-tilt room-temperature holder were tilted at angles ranging from −60° to 60° in steps of 2° for the PLTP specimen and −62° to 67° in steps of 1.5° for the PLTP-HDL3 specimen. The total illumination electron dose was ~200 $e^-/Å^2$. The tilt series of tomographic data were controlled and imaged by manual operation with the Gatan tomography software (Zeiss Libra 120 TEM) and automated tomography software preinstalled in the microscopes [67]. Collected micrographs were initially aligned together following the procedure of the IMOD

software package [68]. The tilt series of each particle image in windows of 220 × 220 pixels (PLTP) and 256 × 256 pixels (PLTP-HDL_3) were semi-automatically tracked and selected by the IPET software. The defocus of the small particle image area of each tilt micrograph was examined by fitting the CTF parameters with its power spectrum by *ctffind3* in the FREALIGN software package [69]. The CTF was then corrected by TOMOCTF [70].

4.5. Individual particle electron tomography (IPET) 3D reconstruction

The 3D density maps of an individual PLTP and PLTP-HDL_3 complex were reconstructed by the IPET method [42]. In brief, a small image area containing only a single PLTP particle and PLTP-HDL_3 complex particle were windowed from each tilted whole-micrograph after CTF correction. An ab-initio model was generated by directly back-projecting these small images into a 3D map. The map was then refined via three rounds of refinement loops (including more than a hundred iterations) by the focused electron tomography reconstruction (FETR) algorithm [42]. In FETR, an automatically generated dynamic Gaussian low-pass filter and an automatically generated soft-mask were applied to both the references and tilted images to achieve the final 3D reconstruction. To analyze tomographic 3D reconstructions, the center-refined raw ET images were split into two groups based on having an odd- or even-numbered index in the order of tilt angles [42]. The frequency at which the intra-FSC curve falls to a value of 0.5 showed that the resolutions of the reconstruction density maps of the PLTP and PLTP-HDL_3 particles are in the range of ~19–27 Å. A 3D IPET density map from the IPET reconstruction was low pass filtered to 80 Å, which prepared for the initial model for single particle reconstruction.

4.6. Single particle 3D reconstruction of PLTP and PLTP-HDL_3 particles

Approximately 7000 isolated PLTP particles and ~5000 HDL_3-PLTP complexes (from an initial pool of ~32,000 particles) were extracted from the micrographs by using a window of 196 × 196 and 256 × 256 pixel images, respectively, using the *e2boxer.py* program in EMAN2 [71]. The CTF-corrected images of the particles were submitted for reference-free class averaging and approximately 300 class averages were generated for both the PLTP and the PLTP-HDL_3 complex using *refind2d.py* in EMAN [43]. To prevent bias from a given initial model for single particle 3D reconstruction, the IPET 3D reconstructions of the PLTP and the PLTP-HDL_3 complex was filtered to 80 Å and then used as the initial models. According to the 0.5 Fourier shell correlation criterion [72], the final resolutions of the asymmetric reconstructions of the PLTP and the PLTP-HDL_3 complex were 19 Å and 23 Å, respectively. The contour level of the 81 kDa PLTP was estimated from the average density of protein of 1.22 g cm^{-3} [73].

4.7. Statistical analyses of PLTP binding to lipoprotein particles

To harvest a sufficient number of isolated lipoprotein/PLTP particles for statistical analysis, 4–5 images (containing 300–500 particles) were collected from each sample at a given time mentioned above. For the statistic of the percentage of HDL_3 binding to PLTPs, the number of bound PLTPs was counted by accumulating the number of observed rod-shaped protrusions on the edge of the sphere. This number could be slightly different by including the undetectable CETPs that were located behind or in front of the lipoprotein particles. As we previously calculated [22], the probability ($\mathscr{P}$) (i.e., the ratio of the PLTP visible area vs. the overall sphere area) is $\mathscr{P} = cos\left[sin^{-1}\left(\frac{d}{d+2l}\right)\right]$, where d is the lipoprotein diameter and l is the PLTP protrusion length. Since the sizes of HDLs were small, this correction was not significant. The particle diameter and the PLTP protrusion width and length were determined by measuring the diameters in two orthogonal directions, as previously described [22]. In brief, the geometric mean of the two perpendicular diameters was used to represent the particle diameter and the PLTP protrusion geometry.

Conflict of interest

Authors have no conflict of interest.

Transparency document

The Transparency document associated with this article can be found, in online version.

Acknowledgments

We thank Drs. Douglas and Ronald Krauss for providing the HDL_3 and LDL samples. This work was supported by the National Heart, Lung, and Blood Institute of the National Institutes of Health (R01HL115153, R01GM104427, and P01HL030086). Work at the Molecular Foundry was supported by the Office of Science, Office of Basic Energy Sciences of the U.S. Department of Energy under Contract No. DE-AC02-05CH11231.

Author contributions

This project was initiated and designed by SV and GR. MZ conducted the experiments and acquired the OpNS data. MZ processed the NS data and computed the statistics. MZ and XZ reconstructed the 3D IPET. MZ drafted the initial manuscript, which was revised by JJA, SV and GR.

Appendix A. Supplementary data

Supplementary data to this article can be found online at https://doi.org/10.1016/j.bbalip.2018.06.001.

References

[1] R. Rao, J.J. Albers, G. Wolfbauer, H.J. Pownall, Molecular and macromolecular specificity of human plasma phospholipid transfer protein, Biochemistry 36 (1997) 3645–3653.
[2] A.R. Tall, S. Krumholz, T. Olivecrona, R.J. Deckelbaum, Plasma phospholipid transfer protein enhances transfer and exchange of phospholipids between very low density lipoproteins and high density lipoproteins during lipolysis, J. Lipid Res. 26 (1985) 842–851.
[3] M. Jauhiainen, J. Metso, R. Pahlman, S. Blomqvist, A. van Tol, C. Ehnholm, Human plasma phospholipid transfer protein causes high density lipoprotein conversion, J. Biol. Chem. 268 (1993) 4032–4036.
[4] B.F. Asztalos, H.D.L.A.T. Study, High-density lipoprotein metabolism and progression of atherosclerosis: new insights from the HDL Atherosclerosis Treatment Study, Curr. Opin. Cardiol. 19 (2004) 385–391.
[5] J.F. Oram, G. Wolfbauer, C. Tang, W.S. Davidson, J.J. Albers, An amphipathic helical region of the N-terminal barrel of phospholipid transfer protein is critical for ABCA1-dependent cholesterol efflux, J. Biol. Chem. 283 (2008) 11541–11549.
[6] A. Schlitt, C. Bickel, P. Thumma, S. Blankenberg, H.J. Rupprecht, J. Meyer, X.C. Jiang, High plasma phospholipid transfer protein levels as a risk factor for coronary artery disease, Arterioscl. Throm. Vas. 23 (2003) 1857–1862.
[7] C. Bickel, P. Thumma, S. Blankenberg, H.J. Rupprecht, A. Schlitt, J. Meyer, X.C. Jiang, High plasma phospholipid transfer protein (PLTP) levels as a risk factor for coronary artery disease, Circulation 106 (2002) 45-45.
[8] X.Y. Chen, A.J. Sun, A. Mansoor, Y.Z. Zou, J.B. Ge, J.M. Lazar, X.C. Jiang, Plasma PLTP activity is inversely associated with HDL-C levels, Nutr. Metab. 6 (2009).
[9] A. Schlitt, S. Blankenberg, C. Bickel, K.J. Lackner, G.H. Heine, M. Buerke, K. Werdan, L. Maegdefessel, U. Raaz, H.J. Rupprecht, T. Munzel, X.C. Jiang, PLTP activity is a risk factor for subsequent cardiovascular events in CAD patients under statin therapy: the AtheroGene Study, J. Lipid Res. 50 (2009) 723–729.
[10] W. Schgoer, T. Mueller, M. Jauhiainen, A. Wehinger, R. Gander, I. Tancevski, K. Salzmann, P. Eller, A. Ritsch, M. Haltmayer, C. Ehnholm, J.R. Patsch, B. Foeger, Low phospholipid transfer protein (PLTP) is a risk factor for peripheral atherosclerosis, Atherosclerosis 196 (2008) 219–226.
[11] R.J. Liu, M.R. Hojjati, C.M. Devlin, I.H. Hansen, X.C. Jiang, Macrophage phospholipid transfer protein deficiency and ApoE secretion - impact on mouse plasma cholesterol levels and atherosclerosis, Arterioscl. Throm. Vas. 27 (2007) 190–196.
[12] J.R. Day, J.J. Albers, C.E. Lofton-Day, T.L. Gilbert, A.F. Ching, F.J. Grant, P.J. O'Hara, S.M. Marcovina, J.L. Adolphson, Complete cDNA encoding human

phospholipid transfer protein from human endothelial cells, J. Biol. Chem. 269 (1994) 9388–9391.
[13] D. Masson, X.C. Jiang, L. Lagrost, A.R. Tall, The role of plasma lipid transfer proteins in lipoprotein metabolism and atherogenesis, J. Lipid Res. 50 (Suppl) (2009) S201–S206.
[14] L.J. Beamer, Structure of human BPI (bactericidal/permeability-increasing protein) and implications for related proteins, Biochem. Soc. Trans. 31 (2003) 791–794.
[15] K. Kawano, S.C. Qin, M. Lin, A.R. Tall, X.C. Jiang, Cholesteryl ester transfer protein and phospholipid transfer protein have nonoverlapping functions in vivo, J. Biol. Chem. 275 (2000) 29477–29481.
[16] R.E. Morton, L. Izem, Modification of CETP function by changing its substrate preference: a new paradigm for CETP drug design, J. Lipid Res. 56 (2015) 612–619.
[17] X.C. Jiang, C. Bruce, J. Mar, M. Lin, Y. Ji, O.L. Francone, A.R. Tall, Targeted mutation of plasma phospholipid transfer protein gene markedly reduces high-density lipoprotein levels, J. Clin. Invest. 103 (1999) 907–914.
[18] K.A. Rye, N.J. Hime, P.J. Barter, Evidence that cholesteryl ester transfer protein-mediated reductions in reconstituted high density lipoprotein size involve particle fusion, J. Biol. Chem. 272 (1997) 3953–3960.
[19] N. Settasatian, M. Duong, L.K. Curtiss, C. Ehnholm, M. Jauhiainen, J. Huuskonen, K.A. Rye, The mechanism of the remodeling of high density lipoproteins by phospholipid transfer protein, J. Biol. Chem. 276 (2001) 26898–26905.
[20] K.A. Rye, N.J. Hime, P.J. Barter, Evidence that cholesteryl ester transfer protein-mediated reductions in reconstituted high density lipoprotein size involve particle fusion, J. Biol. Chem. 272 (1997) 3953–3960.
[21] L. Zhang, F. Yan, S. Zhang, D. Lei, M.A. Charles, G. Cavigiolio, M. Oda, R.M. Krauss, K.H. Weisgraber, K.A. Rye, H.J. Pownall, X. Qiu, G. Ren, Structural basis of transfer between lipoproteins by cholesteryl ester transfer protein, Nat. Chem. Biol. 8 (2012) 342–349.
[22] M. Zhang, R. Charles, H. Tong, L. Zhang, M. Patel, F. Wang, M.J. Rames, A. Ren, K.A. Rye, X. Qiu, D.G. Johns, M.A. Charles, G. Ren, HDL surface lipids mediate CETP binding as revealed by electron microscopy and molecular dynamics simulation, Sci. Rep. 5 (2015) 8741.
[23] M. Zhang, D. Lei, B. Peng, M. Yang, L. Zhang, M.A. Charles, K.A. Rye, R.M. Krauss, D.G. Johns, G. Ren, Assessing the mechanisms of cholesteryl ester transfer protein inhibitors, Biochim. Biophys. Acta 1862 (2017) 1606–1617.
[24] M.E. Lauer, A. Graff-Meyer, A.C. Rufer, C. Maugeais, E. von der Mark, H. Matile, B. D'Arcy, C. Magg, P. Ringler, S.A. Muller, S. Scherer, G. Dernick, R. Thoma, M. Hennig, E.J. Niesor, H. Stahlberg, Cholesteryl ester transfer between lipoproteins does not require a ternary tunnel complex with CETP, J. Struct. Biol. 194 (2016) 191–198.
[25] J. Huuskonen, G. Wohlfahrt, M. Jauhiainen, C. Ehnholm, O. Teleman, V.M. Olkkonen, Structure and phospholipid transfer activity of human PLTP: analysis by molecular modeling and site-directed mutagenesis, J. Lipid Res. 40 (1999) 1123–1130.
[26] C. Bruce, L.J. Beamer, A.R. Tall, The implications of the structure of the bactericidal/permeability-increasing protein on the lipid-transfer function of the cholesteryl ester transfer protein, Curr. Opin. Struct. Biol. 8 (1998) 426–434.
[27] L.J. Beamer, S.F. Carroll, D. Eisenberg, The BPI/LBP family of proteins: a structural analysis of conserved regions, Protein Sci. 7 (1998) 906–914.
[28] X. Qiu, A. Mistry, M.J. Ammirati, B.A. Chrunyk, R.W. Clark, Y. Cong, J.S. Culp, D.E. Danley, T.B. Freeman, K.F. Geoghegan, M.C. Griffor, S.J. Hawrylik, C.M. Hayward, P. Hensley, L.R. Hoth, G.A. Karam, M.E. Lira, D.B. Lloyd, K.M. Mcgrath, K.J. Stutzman-Engwall, A.K. Subashi, T.A. Subashi, J.F. Thompson, I.K. Wang, H. Zhao, A.P. Seddon, Crystal structure of cholesteryl ester transfer protein reveals a long tunnel and four bound lipid molecules, Nat. Struct. Mol. Biol. 14 (2007) 106–113.
[29] J. Ihm, D.M. Quinn, S.J. Busch, B. Chataing, J.A. Harmony, Kinetics of plasma protein-catalyzed exchange of phosphatidylcholine and cholesteryl ester between plasma lipoproteins, J. Lipid Res. 23 (1982) 1328–1341.
[30] P.J. Barter, M.E. Jones, Kinetic studies of the transfer of esterified cholesterol between human plasma low and high density lipoproteins, J. Lipid Res. 21 (1980) 238–249.
[31] G. Ren, G. Rudenko, S.J. Ludtke, J. Deisenhofer, W. Chiu, H.J. Pownall, Model of human low-density lipoprotein and bound receptor based on cryoEM, Proc. Natl. Acad. Sci. U. S. A. 107 (2010) 1059–1064.
[32] Y. Yu, Y.L. Kuang, D. Lei, X. Zhai, M. Zhang, R.M. Krauss, G. Ren, Polyhedral 3D structure of human plasma very low density lipoproteins by individual particle cryo-electron tomography1, J. Lipid Res. 57 (2016) 1879–1888.
[33] R. van Antwerpen, M. La Belle, E. Navratilova, R.M. Krauss, Structural heterogeneity of apoB-containing serum lipoproteins visualized using cryo-electron microscopy, J. Lipid Res. 40 (1999) 1827–1836.
[34] L. Zhang, J. Song, G. Cavigiolio, B.Y. Ishida, S. Zhang, J.P. Kane, K.H. Weisgraber, M.N. Oda, K.A. Rye, H.J. Pownall, G. Ren, Morphology and structure of lipoproteins revealed by an optimized negative-staining protocol of electron microscopy, J. Lipid Res. 52 (2011) 175–184.
[35] B. Chen, X. Ren, T. Neville, W.G. Jerome, D.W. Hoyt, D. Sparks, G. Ren, J. Wang, Apolipoprotein AI tertiary structures determine stability and phospholipid-binding activity of discoidal high-density lipoprotein particles of different sizes, Protein Sci. 18 (2009) 921–935.
[36] R.A. Silva, R. Huang, J. Morris, J. Fang, E.O. Gracheva, G. Ren, A. Kontush, W.G. Jerome, K.A. Rye, W.S. Davidson, Structure of apolipoprotein A-I in spherical high density lipoproteins of different sizes, Proc. Natl. Acad. Sci. U. S. A. 105 (2008) 12176–12181.
[37] L. Zhang, J. Song, Y. Newhouse, S. Zhang, K.H. Weisgraber, G. Ren, An optimized negative-staining protocol of electron microscopy for apoE4 POPC lipoprotein, J. Lipid Res. 51 (2010) 1228–1236.
[38] L. Zhang, H. Tong, M. Garewal, G. Ren, Optimized negative-staining electron microscopy for lipoprotein studies, Biochim. Biophys. Acta 1830 (2013) 2150–2159.
[39] H. Tong, L. Zhang, A. Kaspar, M.J. Rames, L. Huang, G. Woodnutt, G. Ren, Peptide-conjugation induced conformational changes in human IgG1 observed by optimized negative-staining and individual-particle electron tomography, Sci. Rep. Uk 3 (2013) 1089.
[40] L. Zhang, D.S. Lei, J.M. Smith, M. Zhang, H.M. Tong, X. Zhang, Z.Y. Lu, J.K. Liu, A.P. Alivisatos, G. Ren, Three-dimensional structural dynamics and fluctuations of DNA-nanogold conjugates by individual-particle electron tomography, Nat. Commun. 7 (2016).
[41] M. Rames, Y. Yu, G. Ren, Optimized negative staining: a high-throughput protocol for examining small and asymmetric protein structure by electron microscopy, J. Vis. Exp. (2014) e51087.
[42] L. Zhang, G. Ren, IPET and FETR: experimental approach for studying molecular structure dynamics by cryo-electron tomography of a single-molecule structure, PLoS One 7 (2012) e30249.
[43] S.J. Ludtke, P.R. Baldwin, W. Chiu, EMAN: semiautomated software for high-resolution single-particle reconstructions, J. Struct. Biol. 128 (1999) 82–97.
[44] C. Desrumaux, C. Labeur, A. Verhee, J. Tavernier, J. Vandekerckhove, M. Rosseneu, F. Peelman, A hydrophobic cluster at the surface of the human plasma phospholipid transfer protein is critical for activity on high density lipoproteins, J. Biol. Chem. 276 (2001) 5908–5915.
[45] J.F. Oram, G. Wolfbauer, C. Tang, W.S. Davidson, J.J. Albers, An amphipathic helical region of the N-terminal barrel of phospholipid transfer protein is critical for ABCA1-dependent cholesterol efflux, J. Biol. Chem. 283 (2008) 11541–11549.
[46] V.R. Chirasani, P.D. Revanasiddappa, S. Senapati, Structural plasticity of cholesteryl ester transfer protein assists the lipid transfer activity, J. Biol. Chem. 291 (2016) 19462–19473.
[47] E.F. Pettersen, T.D. Goddard, C.C. Huang, G.S. Couch, D.M. Greenblatt, E.C. Meng, T.E. Ferrin, UCSF chimera–a visualization system for exploratory research and analysis, J. Comput. Chem. 25 (2004) 1605–1612.
[48] A. Korhonen, M. Jauhiainen, C. Ehnholm, P.T. Kovanen, M. Ala-Korpela, Remodeling of HDL by phospholipid transfer protein: demonstration of particle fusion by 1H NMR spectroscopy, Biochem. Biophys. Res. Commun. 249 (1998) 910–916.
[49] J. Damen, J. Regts, G. Scherphof, Transfer of [14C]phosphatidylcholine between liposomes and human plasma high density lipoprotein. Partial purification of a transfer-stimulating plasma factor using a rapid transfer assay, Biochim. Biophys. Acta 712 (1982) 444–452.
[50] M.C. Cheung, G. Wolfbauer, J.J. Albers, Plasma phospholipid mass transfer rate: relationship to plasma phospholipid and cholesteryl ester transfer activities and lipid parameters, Biochim. Biophys. Acta 1303 (1996) 103–110.
[51] T. Oka, T. Kujiraoka, M. Ito, T. Egashira, S. Takahashi, M.N. Nanjee, N.E. Miller, J. Metso, V.M. Olkkonen, C. Ehnholm, M. Jauhiainen, H. Hattori, Distribution of phospholipid transfer protein in human plasma: presence of two forms of phospholipid transfer protein, one catalytically active and the other inactive, J. Lipid Res. 41 (2000) 1651–1657.
[52] M.T. Janis, S. Siggins, E. Tahvanainen, R. Vikstedt, K. Silander, J. Metso, A. Aromaa, M.R. Taskinen, V.M. Olkkonen, M. Jauhiainen, C. Ehnholm, Active and low-active forms of serum phospholipid transfer protein in a normal Finnish population sample, J. Lipid Res. 45 (2004) 2303–2309.
[53] M.C. Cheung, G. Wolfbauer, J.J. Albers, Different phospholipid transfer protein complexes contribute to the variation in plasma PLTP specific activity, Biochim. Biophys. Acta 1811 (2011) 343–347.
[54] P.J. Pussinen, M. Jauhiainen, J. Metso, L.E. Pyle, Y.L. Marcel, N.H. Fidge, C. Ehnholm, Binding of phospholipid transfer protein (PLTP) to apolipoproteins A-I and A-II: location of a PLTP binding domain in the amino terminal region of apoA-I, J. Lipid Res. 39 (1998) 152–161.
[55] P.J. Pussinen, M. Jauhiainen, C. Ehnholm, ApoA-II/apoA-I molar ratio in the HDL particle influences phospholipid transfer protein-mediated HDL interconversion, J. Lipid Res. 38 (1997) 12–21.
[56] M. Rosseneu, P. Tornout, M.-J. Lievens, G. Assmann, Displacement of the Human Apoprotein A-I by the Human Apoprotein A-II from Complexes of (Apoprotein A-I)-Phosphatidylcholine-Cholesterol, FEBS J. 117 (1981) 347–352.
[57] N.L. Setala, J.M. Holopainen, J. Metso, S.K. Wiedmer, G. Yohannes, P.K. Kinnunen, C. Ehnholm, M. Jauhiainen, Interfacial and lipid transfer properties of human phospholipid transfer protein: implications for the transfer mechanism of phospholipids, Biochemistry 46 (2007) 1312–1319.
[58] J.J. Albers, S. Vuletic, M.C. Cheung, Role of plasma phospholipid transfer protein in lipid and lipoprotein metabolism, Biochim. Biophys. Acta 1821 (2012) 345–357.
[59] Y.D. Yu, Y.L. Kuang, D.S. Lei, X.B. Zhai, M. Zhang, R.M. Krauss, G. Ren, Polyhedral 3D structure of human plasma very low density lipoproteins by individual particle cryo-electron tomography, J. Lipid Res. 57 (2016) 1879–1888.
[60] J.J. Albers, G. Wolfbauer, M.C. Cheung, J.R. Day, A.F. Ching, S. Lok, A.Y. Tu, Functional expression of human and mouse plasma phospholipid transfer protein: effect of recombinant and plasma PLTP on HDL subspecies, Biochim. Biophys. Acta 1258 (1995) 27–34.
[61] J.J. Albers, J.R. Day, G. Wolfbauer, H. Kennedy, S. Vuletic, M.C. Cheung, Impact of site-specific N-glycosylation on cellular secretion, activity and specific activity of the plasma phospholipid transfer protein, Biochim. Biophys. Acta 1814 (2011) 908–911.
[62] S. Han, A.M. Flattery, D. McLaren, R. Raubertas, S.H. Lee, V. Mendoza, R. Rosa, N. Geoghagen, J.M. Castro-Perez, T.P. Roddy, G. Forrest, D. Johns, B.K. Hubbard, J. Li, Comparison of lipoprotein separation and lipid analysis methodologies for human and cynomolgus monkey plasma samples, J. Cardiovasc. Transl. Res. 5 (2012) 75–83.

[63] M.P. Caulfield, S. Li, G. Lee, P.J. Blanche, W.A. Salameh, W.H. Benner, R.E. Reitz, R.M. Krauss, Direct determination of lipoprotein particle sizes and concentrations by ion mobility analysis, Clin. Chem. 54 (2008) 1307–1316.
[64] M. Ohi, Y. Li, Y. Cheng, T. Walz, Negative staining and image classification - powerful tools in modern electron microscopy, Biol. Proced. Online 6 (2004) 23–34.
[65] N. Grigorieff, FREALIGN: high-resolution refinement of single particle structures, J. Struct. Biol. 157 (2007) 117–125.
[66] J. Frank, M. Radermacher, P. Penczek, J. Zhu, Y.H. Li, M. Ladjadj, A. Leith, SPIDER and WEB: processing and visualization of images in 3D electron microscopy and related fields, J. Struct. Biol. 116 (1996) 190–199.
[67] J. Liu, H. Li, L. Zhang, M. Rames, M. Zhang, Y. Yu, B. Peng, C.D. Celis, A. Xu, Q. Zou, X. Yang, X. Chen, G. Ren, Fully mechanically controlled automated electron microscopic tomography, Sci. Rep. 6 (2016) 29231.
[68] J.R. Kremer, D.N. Mastronarde, J.R. Mcintosh, Computer visualization of three-dimensional image data using IMOD, J. Struct. Biol. 116 (1996) 71–76.
[69] N. Grigorieff, FREALIGN: high-resolution refinement of single particle structures, J. Struct. Biol. 157 (2007) 117–125.
[70] J.J. Fernandez, S. Li, R.A. Crowther, CTF determination and correction in electron cryotomography, Ultramicroscopy 106 (2006) 587–596.
[71] G. Tang, L. Peng, P.R. Baldwin, D.S. Mann, W. Jiang, I. Rees, S.J. Ludtke, EMAN2: an extensible image processing suite for electron microscopy, J. Struct. Biol. 157 (2007) 38–46.
[72] B. Bottcher, S.A. Wynne, R.A. Crowther, Determination of the fold of the core protein of hepatitis B virus by electron cryomicroscopy, Nature 386 (1997) 88–91.
[73] K.M. Andersson, S. Hovmoller, The protein content in crystals and packing coefficients in different space groups, Acta Crystallogr. D Biol. Crystallogr. 56 (2000) 789–790.